This MICCAI paper is the Open Access version, provided by the MICCAI Society. It is identical to the accepted version, except for the format and this watermark; the final published version is available on SpringerLink.

Vision-Based Force Estimation Using Brain Surface Deformation Models

Chakib Heraoui[1,3], Nazim Haouchine[2], Nazim Ouadahi[3], Amir Hooshiar[4], D. Louis Collins[4], Rolando F. Del Maestro[5], and Houssem-Eddine Gueziri[1,4]*

[1] Université TÉLUQ, Montreal, QC, Canada, houssem.gueziri@teluq.ca
[2] Harvard Medical School, Brigham and Women's Hospital, Boston, USA
[3] École Supérieure des Sciences et Technologies, Algiers 16104, Algeria
[4] McGill University, Montreal, QC, Canada
[5] Neurosurgical Simulation and Artificial Intelligence Learning Centre, Montreal, QC, Canada

Abstract. Haptic feedback is critical for neurosurgical training simulators, yet measuring contact forces in soft tissue interaction remains challenging. This paper presents a deep learning framework that estimates tool-tissue interaction forces directly from brain surface deformations captured by a monocular surgical microscope. A realistic dataset was generated using finite element method simulation in SOFA. The dataset contains ground-truth force magnitudes derived from tool-tissue interactions in neurosurgical scenarios. We developed D2FNet, a multi-scale convolutional neural network trained using a novel anti-ghost loss function that incorporates an asymmetric weighting scheme applying a penalty to over-predictions in low-force regions. This minimizes false high-force estimates likely to induce erroneous haptic responses. The model processes spatial features from normalized displacements, magnitude, brain mask, and divergence field. Our method enables non-invasive estimation of interaction forces using only 2D video sequences. Cross-validation on simulated data achieved R^2=0.788±0.039 and mean absolute error (MAE)=6.4±0.8 mN. The anti-ghost loss reduced spurious force predictions by 73% compared to standard MSE training, particularly in low-force regions. We demonstrate feasibility through an ex vivo calf brain experiment and quantitatively compare estimated global forces with ground-truth measurements from an external force sensor. Results showed good agreement between the predicted forces and ground-truth measurements (MAE=0.071 N, Corr.=71.1%). Frame-independent force estimation from monocular surface deformation is feasible and clinically relevant for real-time force feedback rendering in realistic surgical simulators, with potential applications in intraoperative force monitoring.

Keywords: Neurosurgery simulation · Force estimation · Deep learning · Finite element method · Brain biomechanics · Surgical training

1 Introduction

Neurosurgical procedures require extreme precision due to the delicate nature of brain tissue. Excessive tool-tissue contact forces can cause irreversible injury, while insufficient contact limits surgical performance. Cadaveric studies with force-sensing bipolar forceps have shown that neurosurgical forces are remarkably low with maximal peak at 1.35 N, and over 70% of measured forces fall below 0.3 N [4]. Yet, force application remains a largely qualitative skill taught through years of apprenticeship. Haptic-enabled virtual surgery simulations offer risk-free training environments, but require accurate force models for realistic feedback [10, 12], and animal-based simulation models [18, 16, 1] lack the quantitative force feedback needed to develop advanced tactile skills.

Early neurosurgical force sensing used strain gauge–based tools [4], requiring specialized hardware and calibration, and cannot estimate forces in purely computational simulations where only virtual deformation is available. Software-based approaches instead use biomechanical modeling with FEM, such as the SOFA framework [3], which enables real-time simulation using experimentally validated brain tissue properties [7, 2]. However, FEM methods solve the forward problem—computing deformation from known forces—rather than the inverse problem of inferring forces from observed deformations, which requires accurate material parameters and limits real-time inverse force estimation. Vision-based deep learning methods offer a promising alternative [9], but have been mainly validated on silicone phantoms rather than brain tissue. In this work, we focus on force estimation for ex vivo neurosurgical training, where biological tissue specimens are used as physical models to replicate surgical manipulation in a controlled setting. We propose a data-driven method that predicts spatially resolved contact forces directly from 2D surface displacement fields captured by standard surgical microscopes, using FEM-based brain tissue simulations to train convolutional neural networks for the inverse deformation-to-force mapping.

Contribution. Our contributions are three-fold: 1) we introduce a framework for generating visually realistic neurosurgical simulation data with ground-truth force measurements to enable the training and validation of machine learning models; 2) we introduce a novel Anti-Ghost Loss Function with asymmetric penalty for over-predictions in low-force regions, directly addressing surgical safety requirements where false positive high forces could lead to tissue damage; 3) we develop D2FNet with pyramid pooling, attention mechanisms, and divergence field features that capture tissue compression patterns, enabling accurate force prediction across diverse surgical scenarios. The neurosurgical force data generation methods in the SOFA simulation framework[6], as well as all trained models[7] are publicly available.

2 Methods

Brain Biomechanical Modeling: The brain was modeled using a co-rotational finite element method (FEM), in which the stress–strain relationship is evaluated locally within each element's own reference frame, keeping the constitutive

[6] Data generation: https://github.com/D3MIA/SOFA-NeuroSim-Recorder
[7] Force estimation: https://github.com/D3MIA/D2FNet

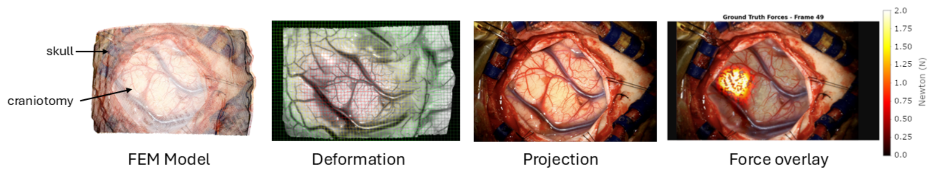

Fig. 1. Illustration of the proposed data generation framework, from left to right: FEM model is used to to simulate brain tissue biomechanics, forces are applied generating deformations, which are projected on camera view to produce 2D displacement fields, along with corresponding ground truth force maps.

behavior linear while rigid-body rotations and geometric nonlinearities are handled globally through continuous frame updates. This formulation thus captures large deformations without requiring a fully nonlinear material model, offering a computationally efficient alternative to nonlinear viscoelastic approaches for large-scale dataset generation while still yielding physiologically plausible deformations,[7, 2, 8]. The model includes a 12 mm radius craniotomy and four boundary conditions simulating dura attachments at the falx cerebri and skull. These constraints prevent rigid-body motion while allowing localized deformation within the craniotomy. A linear elastic model was used, with isotropic stress-strain relationship:

$$\boldsymbol{\sigma} = \lambda \mathrm{tr}(\boldsymbol{\epsilon})\mathbf{I} + 2\mu\boldsymbol{\epsilon} \tag{1}$$

where $\boldsymbol{\sigma}$ is the Cauchy stress tensor, $\boldsymbol{\epsilon}$ is the infinitesimal strain tensor, $\mathbf{I}$ is the identity matrix, and $\lambda = \frac{E\nu}{(1+\nu)(1-2\nu)}$ and $\mu = \frac{E}{2(1+\nu)}$ are Lamé parameters derived via standard elasticity relations [15]. Using the DejaVu simulation SOFA plugin [5], tissue deformation was induced by applying spatially distributed forces centered at randomly sampled surface locations within the craniotomy region, producing diverse tissue displacement patterns across the dataset.

Data generation: An overview of the proposed data generation framework is shown in Fig.1. Volumetric reaction forces $\mathbf{f}_j^{\mathrm{vol}}(t) \in \mathbb{R}^3$ were computed at each node of a sparse tetrahedral mesh representing the mechanical response to tool-tissue interaction.[8] These forces were interpolated to the dense surface mesh using k-nearest neighbor (k=8) spatial averaging with inverse distance weighting:

$$\mathbf{f}_i^{\mathrm{surf}}(t) = \sum_{j \in \mathcal{N}_8(i)} w_{ij}\mathbf{f}_j^{\mathrm{vol}}(t), \quad w_{ij} = \frac{d_{ij}^{-1}}{\sum_{j'} d_{ij'}^{-1}} \tag{2}$$

where $d_{ij} = \|\mathbf{x}_i - \mathbf{x}_j\|_2$ is the Euclidean distance between surface node i and volumetric node j, and $\mathcal{N}_8(i)$ denotes the 8 nearest volumetric nodes to surface node i. This scheme ensures spatially smooth force reconstruction while preserving local force gradients at tool contact boundaries.

[8] Forces were extracted from SOFA's constraint solver at each timestamp using a multi-stage pipeline implemented via custom *AnimationRecorder* components.

To simulate computational noise arising during deformation estimation, a two-stage noise injection strategy was implemented. First, Gaussian noise with a constant bias of 0.02 N was introduced at recording time. Second, post-processing geometric noise applied to 5% of low-force surface points far from tool contact, inducing displacement perturbations of $\pm 10\%$ relative to the per-frame displacement range. Finally, force magnitudes $F_i(t) = \|\mathbf{f}_i^{\text{surf}}(t)\|_2$ were projected onto the 2D craniotomy plane via camera transformation matrices.

This complete simulation and projection pipeline generated a comprehensive synthetic dataset with diverse surgical manipulation patterns. The video sequences are composed of repeated single-direction deformation events applied sequentially in different orientations, which closely resemble the pulling actions commonly performed with forceps during surgical interventions.

D2FNet Architecture: We developed D2FNet, a multi-scale U-Net [13], to estimate forces from sparse, noisy deformation data (Fig. 2):

1. *Multi-Scale Attention Mechanisms.* We integrated spatial and channel attention modules [11] at 9 network levels (encoder stages 1–4, bottleneck, decoder stages 1–4). At each decoder level, dual attention gates compute spatial attention $\alpha_{\text{spatial}} = \sigma(W_s * \text{Conv}(x))$ and channel attention $\alpha_{\text{channel}} = \sigma(W_c * \text{GlobalPool}(x))$, with combined weighting $x_{\text{out}} = x \odot \alpha_{\text{spatial}} \odot \alpha_{\text{channel}}$ applied before feature concatenation. This enables selective focus on force-relevant spatial regions while suppressing background noise.

2. *Pyramid Pooling Bottleneck.* We use pyramid pooling at 4 spatial scales [1×1, 2×2, 4×4, 8×8] to capture contextual information [20], enabling the network to integrate local force gradients and global deformation patterns.

3. *Multi-Head Adaptive Fusion.* We employed three specialized prediction heads targeting low (0–0.5 N), medium (0–1.5 N), and high (0–3.0 N) force regimes. Each head produces sigmoid-bounded predictions that are combined via attention-based soft weighting learned during training to optimally fuse predictions across force magnitudes, ensuring non-negative force outputs.

The network takes 256×256 pixel grids with five input channels derived from bilinearly interpolated 2D surface displacements from video, and predicts a single-channel map corresponding to the total 3D force magnitude rather than only the in-plane force component. The input channels encode: 1) normalized d_x/s_x and d_y/s_y displacements, with s_x, s_y as training-set 99.9th percentiles. 2) displacement magnitude $\sqrt{d_x^2 + d_y^2}/s_x$ clipped to [0, 5], where we intentionally use s_x rather than a separate magnitude scale to extend the dynamic range for large deformations while preventing outlier influence, 3) binary brain mask to exclude regions outside craniotomy, and 4) divergence field $\nabla \cdot \mathbf{d} = \frac{\partial d_x}{\partial x} + \frac{\partial d_y}{\partial y}$ computed via finite-difference on Gaussian-smoothed displacement fields (σ=1.0 pixel). Divergence encodes tissue volume changes, distinguishing compressive (negative) from tensile (positive) deformation patterns correlated to force distribution.

Anti-Ghost Loss Function: Standard regression losses (MSE, MAE) treat

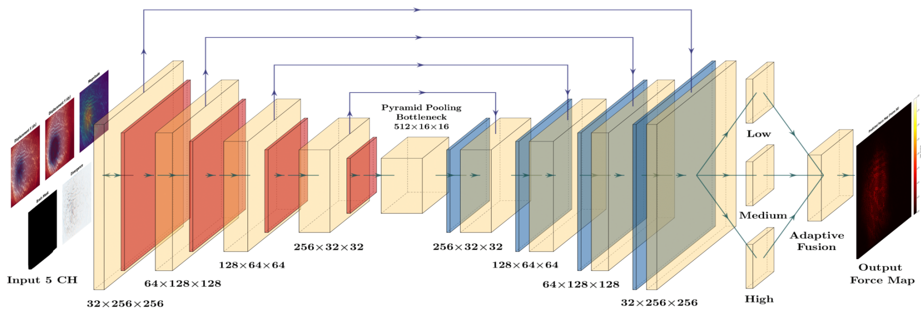

Fig. 2. D2FNet architecture overview. The network takes a 5-channel input (normalized d_x, d_y, magnitude, brain mask, divergence) processed by a U-Net encoder-decoder with pyramid pooling. Three heads predict low (0–0.5N), medium (0–1.5N), and high (0–3.0 N) force ranges, fused via adaptive attention to produce the final 1×256×256 force map. Skip connections preserve spatial detail across scales.

over-predictions and under-predictions symmetrically. In surgical applications, false high forces are considered more harmful than missed low forces. Haptic devices rendering these *phantom* forces may train surgeons to apply excessive pressure, potentially causing tissue damage. We designed an *asymmetric anti-ghost loss* with 3 times stronger penalty for over-predictions in low-force frames, inspired by focal loss for hard example mining [6]:

$$\mathcal{L}_{\text{ghost}} = \frac{1}{N} \sum_{i=1}^{N} w_i \cdot (F_i^{\text{pred}} - F_i^{\text{true}})^2 \tag{3}$$

where weights w_i are defined as:

$$w_i = \begin{cases} 3.0 & \text{if } \bar{F}_{\text{frame}} < \tau \text{ and } F_i^{\text{pred}} > F_i^{\text{true}} \\ 1.0 & \text{otherwise} \end{cases} \tag{4}$$

with frame mean force $\bar{F}_{\text{frame}} = \frac{1}{N} \sum_{i=1}^{N} F_i^{\text{true}}$ and threshold τ=0.05 N.

Finally, we use a linear weighted combination of R^2 objective function and ghost penalty:

$$\mathcal{L}_{\text{total}} = \lambda_{R^2} \cdot \mathcal{L}_{R^2} + \lambda_{ghost} \cdot \mathcal{L}_{\text{ghost}}, \tag{5}$$

where $\mathcal{L}_{R^2} = 1 - R^2$, $R^2 = 1 - \frac{\sum (F_i^{\text{pred}} - F_i^{\text{true}})^2}{\sum (F_i^{\text{true}} - \bar{F})^2}$ and λ_{R^2} and λ_{ghost} are hyperparameters controlling the relative weighting of each term with $\lambda_{R^2} + \lambda_{ghost} = 1$.

Training, Validation and Hyper-parametrization: The network was trained on an NVIDIA A100 GPU (40GB) using the AdamW optimizer with weight decay $\lambda = 10^{-5}$ and initial learning rate 5×10^{-4}, reduced by 0.5 upon validation plateau (patience=5). A batch size of 8 was used due to memory constraints, with gradient clipping (max norm=1.0) for stability. Each fold was trained for

Table 1. Cross-validation results on simulated data.

Metric	Fold 1	Fold 2	Fold 3	**Mean ± SD**	**Coeff. of variation**
R^2 Score	0.756	0.843	0.765	0.788 ± 0.039	4.97%
MAE (mN)	7.1	5.3	6.8	6.4 ± 0.8	12.5%
RMSE (mN)	10.3	8.1	9.8	9.4 ± 0.9	9.6%

MAE: mean absolute error; RMSE: root mean square error; mN: millinewton.

50 epochs, saving the best model based on validation R^2. We performed 3-fold cross-validation at the scenario level (26,000 frames training, 12,000 frames validation). Data generation used a volumetric mesh of ∼4096 tetrahedral elements and 40,652 surface nodes for force measurement. Young's modulus was set to $E = 500$ Pa and Poisson's ratio to $\nu = 0.4$, consistent with reported brain tissue properties at low strain rates [14, 19]. Total tissue mass was 1.0 kg. Velocity-proportional damping (coefficient 2.0) ensured numerical stability and convergence. Lamé parameters were $\lambda = 714.29$ Pa and $\mu = 178.57$ Pa [15].

Experiment: We conducted a feasibility study on an ex vivo calf brain to evaluate applicability under more realistic conditions. The brain was manipulated with bipolar forceps while an external force sensor (SensONE, Bota Systems, Zürich, Switzerland) continuously measured the resulting ground truth forces. Synchronized videos were recorded with an endoscopic camera at 23 fps and 680 × 480 resolution. To mitigate instrument-induced occlusions, the forceps were manually segmented on each frame and inpainted using mean intensity. Dense tissue deformation was then estimated using frame-to-frame total variation registration method [17] with 6 pyramid levels and 0.3 grid regularization factor. Pixel-to-millimeter conversion was obtained by comparing small displacements of tracked forceps measured with an external optical tracking system (Polaris VEGA, Northern Digital Inc., ON, Canada) to corresponding tool motion in the video, assuming a camera axis normal to the brain surface. The resulting deformations were provided as inputs to the proposed model to predict the applied forces, which were then compared with the ground-truth sensor measurements.

3 Results

Table 1 summarizes cross-validation results. The method achieved consistent R^2 score ranging [0.756–0.843]) with mean 0.788±0.039 and MAE=6.4±0.8 mN. The low coefficient of variation (CV=4.97%) demonstrates good model stability and reproducibility across surgical scenarios. To evaluate the anti-ghost loss, we conducted an ablation study by training a baseline model with standard MSE on Fold 2 using identical settings. Anti-ghost loss reduced false positives by 73% (31.2%→8.4%) and mean over-prediction by 73% (18.4→4.9 mN) in low-force frames, while improving R^2 by +2.7% (0.821→0.843), suggesting asymmetric penalties improve safety-critical force prediction for haptic rendering.

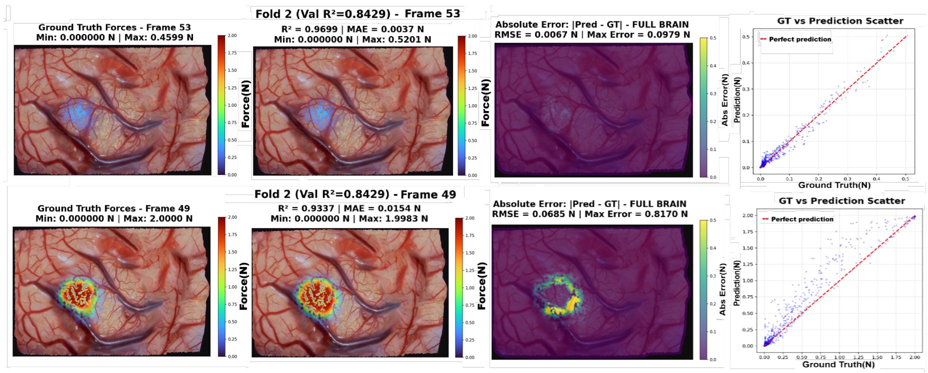

Fig. 3. Qualitative results: on low-force palpation scenario (top) and on high-force retraction scenario (bottom). From left to right: ground-truth, predicted, absolute error and scatter plots of ground truth vs. predicted forces.

Figure 3 shows qualitative performance on representative validation frames across different force regimes. Top row shows results for a low-force palpation (peak 0.46 N). Despite reduced force, the model remains highly accurate (R^2=0.970, MAE=3.7 mN) with good spatial localization of the contact region and low absolute error (RMSE 6.7 mN, max error 98 mN). Bottom row shows high-force retraction scenario (peak 2.0 N), where the model demonstrates near-perfect spatial agreement (R^2=0.934, MAE=15.4 mN). The predicted force map accurately captures the contact hotspot's extent and magnitude. The absolute error map shows errors concentrated near force gradient boundaries, with minimal error in uniform force regions. The scatter plot shows strong linear correlation over the full magnitude range with little systematic bias.

Figure 4 shows the results of the ex vivo experiment. We achieved 0.076 N MAE, 0.108 N RMSE, and 71.1% correlation between the estimated and ground-truth forces. The estimated displacement fields exhibit good spatial consistency (Figs 4.c and d). Errors increase near image boundaries as the instrument enters or leaves the field of view, causing occlusions and misregistration.

4 Discussion

The ex vivo calf brain experiment demonstrated promising results, with a strong correlation between the estimated forces and the force sensor measurements. The MAE of 0.076 N represent less than 5.7% of typical neurosurgical peak forces 1.35 N [4], approaching the perceptual threshold for haptic rendering systems. However, the current implementation still requires further improvement. In particular, instrument segmentation was performed manually, and the image registration approach does not yet support real-time processing, which limits immediate clinical applicability.

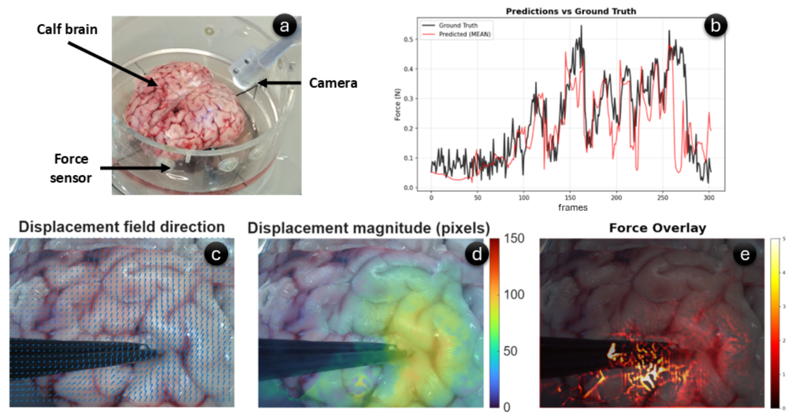

Fig. 4. Ex vivo experiment: (a) experimental setup, (b) predicted force (red) vs. ground-truth sensor measurement (black), (c) estimated displacement field directions, (d) displacement field magnitude, (e) overlay of force predictions.

The frame-independent design processes each timestamp without temporal history, enabling deployment in real-time systems without frame buffering. This approach is justified by the rest-state displacement representation, in which each frame contains complete geometric information and implicitly encodes temporal coherence through the recovered tissue deformation field. Nevertheless, incorporating explicit temporal modeling could further improve prediction stability and temporal consistency across consecutive frames. Incorporating spatial divergence in the input provides explicit encoding of tissue compression/expansion patterns that complement raw displacement information. The model achieved good stability and robustness in simulated data. The proposed approach shows promise across neurosurgical applications. It could improve surgical training simulators with real-time, high-fidelity haptic feedback from optical motion data, support intraoperative monitoring via quantitative video-based force visualization to prevent excessive tissue manipulation, and enable patient-specific planning through fine-tuning on individualized FEM simulations.

Limitations: This study has several limitations related to biomechanical realism, generalization, sensing, and clinical deployment. Training data were generated using finite element simulations with simplified linear elastic properties, which do not fully capture the nonlinear, viscoelastic, anisotropic, and patient-specific behavior of real brain tissue or physiological responses such as inflammation or vascular changes. The model was also evaluated using a single force application pattern and tissue stiffness, limiting generalization to other instruments, interaction modes, and anatomical variability, although the framework can accommodate more diverse training data. Additionally, the monocular 2D approach estimates only force magnitude and does not capture the full 3D force vector. Finally, although force prediction can be run in real time, the current end-to-end pipeline is not fully automated: instrument segmentation and displacement estimation still need manual input and extra computation. More validation is needed in real surgical conditions, including occlusions, lighting changes, and camera motion.

5 Conclusion

We presented a complete framework, from data generation to tool-tissue contact force estimation, for monocular neurosurgical microscope. We achieved clinically relevant accuracy (R^2=0.788, MAE=6.4 mN) on simulated data through a multi-scale U-Net architecture with anti-ghost loss function and divergence field features. The asymmetric penalty approach reduced false high-force predictions by 73%, directly addressing surgical safety requirements for haptic rendering applications. Preliminary results on an ex vivo brain showed good agreement between the predicted forces and the ground-truth sensor measurements, with an MAE of 0.071 N and a correlation of 71.1%. Future work will focus on validating the framework on additional ex vivo surgical data and expanding the dataset to include diverse tissue properties and instrument geometries, enabling broader coverage of clinically representative neurosurgical scenarios.

Acknowledgments. This work was funded by grants from The Canadian Institutes of Health Research (CIHR 195899). C. Heraoui received support through Mitacs Globalink Research Award (IT 45437). N. Haouchine was supported by the Grants from NIH (K25EB035166 and R03EB033910).

Disclosure of Interests. The authors declare that they have no competing interests.

References

1. Almansouri, A., Abou Hamdan, N., Yilmaz, R., Tee, T., Pachchigar, P., Eskandari, M., Agu, C., Giglio, B., Balasubramaniam, N., Bierbrier, J., Collins, D.L., Gueziri, H.E., Del Maestro, R.F.: Continuous instrument tracking in a cerebral corticectomy ex vivo calf brain simulation model: Face and content validation. Operative Neurosurgery **27**(1), 106–113 (2024)
2. Budday, S., Sommer, G., Birkl, C., Langkammer, C., Haybaeck, J., Kohnert, J., Bauer, M., Paulsen, F., Steinmann, P., Kuhl, E., Holzapfel, G.A.: Mechanical characterization of human brain tissue. Acta Biomaterialia **48**, 319–340 (2017)
3. Faure, F., Duriez, C., Delingette, H., Allard, J., Gilles, B., Marchesseau, S., Talbot, H., Courtecuisse, H., Bousquet, G., Peterlik, I., Cotin, S.: SOFA: A multi-model framework for interactive physical simulation. In: Soft Tissue Biomechanical Modeling for Computer Assisted Surgery, Studies in Mechanobiology, Tissue Engineering and Biomaterials, vol. 11, pp. 283–321. Springer, Berlin, Heidelberg (2012)
4. Gan, L.S., Zareinia, K., Lama, S., Maddahi, Y., Yang, F.W., Sutherland, G.R.: Quantification of forces during a neurosurgical procedure: A pilot study. World Neurosurgery **84**(2), 537–548 (2015)
5. Haouchine, N., Stoyanov, D., Roy, F., Cotin, S.: DejaVu: Intra-operative simulation for surgical gesture rehearsal. In: Medical Image Computing and Computer Assisted Intervention – MICCAI 2017. Lecture Notes in Computer Science, vol. 10434, pp. 523–531. Springer, Cham (2017)

6. Lin, T.Y., Goyal, P., Girshick, R., He, K., Dollár, P.: Focal loss for dense object detection. In: 2017 IEEE International Conference on Computer Vision (ICCV). pp. 2999–3007 (2017)
7. Miller, K., Chinzei, K., Orssengo, G., Bednarz, P.: Mechanical properties of brain tissue in-vivo: experiment and computer simulation. Journal of Biomechanics **33**(11), 1369–1376 (2000)
8. Miller, K., Joldes, G.R., Bourantas, G., Warfield, S.K., Hyde, D.E., Kikinis, R., Wittek, A.: Biomechanical modeling and computer simulation of the brain during neurosurgery. International Journal for Numerical Methods in Biomedical Engineering **35**(10), e3250 (2019)
9. Neidhardt, M., Mieling, R., Bengs, M., Schlaefer, A.: Optical force estimation for interactions between tool and soft tissues. Scientific Reports **13**(1), 506 (2023)
10. Okamura, A.M., Verner, L.N., Reiley, C.E., Mahvash, M.: Haptics for robot-assisted minimally invasive surgery. In: Robotics Research, Springer Tracts in Advanced Robotics, vol. 66, pp. 361–372. Springer, Berlin, Heidelberg (2010)
11. Oktay, O., Schlemper, J., Le Folgoc, L., Lee, M., Heinrich, M., Misawa, K., Mori, K., McDonagh, S., Hammerla, N.Y., Kainz, B., Glocker, B., Rueckert, D.: Attention U-Net: Learning where to look for the pancreas. In: Medical Imaging with Deep Learning (2018)
12. Pacchierotti, C., Sinclair, S., Solazzi, M., Frisoli, A., Hayward, V., Prattichizzo, D.: Wearable haptic systems for the fingertip and the hand: Taxonomy, review, and perspectives. IEEE Transactions on Haptics **10**(4), 580–600 (2017)
13. Ronneberger, O., Fischer, P., Brox, T.: U-Net: Convolutional networks for biomedical image segmentation. In: Medical Image Computing and Computer-Assisted Intervention – MICCAI 2015. Lecture Notes in Computer Science, vol. 9351, pp. 234–241. Springer, Cham (2015)
14. Su, L., Qi, B., Yin, J., Qin, X., Genin, G.M., Liu, S., Lu, T.J.: Compressive response of white matter in the brain at low strain-rates. International Journal of Mechanical Sciences **277**, 109415 (2024)
15. Timoshenko, S.P., Goodier, J.N.: Theory of Elasticity. McGraw-Hill, New York, 3rd edn. (1970)
16. Tran, D.H., Winkler-Schwartz, A., Tuznik, M., Gueziri, H.E., Rudko, D.A., Reich, A., Yilmaz, R., Karlik, B., Collins, D.L., Del Maestro, A., Del Maestro, R.F.: Quantitation of tissue resection using a brain tumor model and 7-T magnetic resonance imaging technology. World Neurosurgery **148**, e326–e339 (2021)
17. Vishnevskiy, V., Gass, T., Szekely, G., Tanner, C., Goksel, O.: Isotropic total variation regularization of displacements in parametric image registration. IEEE transactions on medical imaging **36**(2), 385–395 (2016)
18. Winkler-Schwartz, A., Yilmaz, R., Tran, D.H., Gueziri, H.E., Ying, B., Tuznik, M., Fonov, V.S., Collins, D.L., Rudko, D.A., Li, J., Debergue, P., Pazos, V., Del Maestro, R.F.: Creating a comprehensive research platform for surgical technique and operative outcome in primary brain tumor neurosurgery. World Neurosurgery **144**, e62–e71 (2020)
19. Zhang, C., Liu, C., Zhao, H.: Mechanical properties of brain tissue based on microstructure. Journal of the Mechanical Behavior of Biomedical Materials **126**, 104924 (2022)
20. Zhao, H., Shi, J., Qi, X., Wang, X., Jia, J.: Pyramid scene parsing network. In: 2017 IEEE Conference on Computer Vision and Pattern Recognition (CVPR). pp. 2881–2890 (2017)